Frontiers in Scientific Research and Technology

Online ISSN: 2682-2970
Print ISSN: 2682-2962
http://fsrt.journals.ekb.eg

FSRT J 6 (2023) 75 - 91 10.21608/FSRT.2023.209091.1092

Petrogenesis of fractionated calc-alkaline A-type granites and related fluorite, North Eastern Desert, Egypt

Omar Amer[1,*], Sherif Kharbish[2], Ali Maged[2]

[1] Geology Department, Faculty of Science, Zagazig University, Sharkia Governorate, Zagazig 44519, Egypt.

[2] Geology Department, Faculty of Science, Suez University, Suez Governorate, El Salam City, 43518, Egypt.

ARTICLE INFO

Article history:
Received 14 May 2023
Received in revised form 12 June 2023
Accepted 12 June 2023
Available online 15 June 2023

Keywords
Qattar,
Fluorite,
Mineralization,
Hydrothermal,
Granites

ABSTRACT

This study focuses on the petrogenesis of A-type granites and associated fluorite in the Qattar area, Northeastern Desert, Egypt. These granitoids show a geochemical signature typical for an A-type granite, characterized by a slightly peraluminous, highly SiO_2, alkalis (Na_2O+K_2O), U, Rb, Zr, contents, and belong to a group of Ferroan granites with low MgO, CaO, and MnO contents and high FeO^{tot}/ FeO^{tot}+MgO ratios. These rocks emplaced during a late-collisional stage at a temperature of~755.3 °C and pressures from 2.33 to 2.95 kbars under oxidizing conditions (*log* fO_2 -14.85 to -14.91). Moreover, a high 10,000×Ga/Al ratio, negative Eu anomaly, and the tetrad pattern of Qattar alkali–feldspar granites backed up their formation by fractional crystallization and fluid-melt interactions during the late stage of magmatic differentiation. Fluorite mineralization is recorded as four fluorite types (sky blue-, light-yellow-, colorless-, and yellow-type) formed by hydrothermal processes. These fluorites show a wide range of rare earth element variations (∑REE from 76.05 to 166.15) and negative Eu anomaly, which indicates crystallization temperatures above 200 °C. Moreover, Gd / Yb ratios are < 1 in sky blue and light-yellow fluorite and >1 in colorless and yellow fluorites, reflecting various conditions of REE leaching.

1. Introduction

Most of the northern region of the East African Orogen is covered by the Arabian-Nubian Shield (ANS), which has evolved as a result of a complex amalgamation of intra-oceanic island arcs± oceanic plateaus (880 - 630 Ma, [1]. Three main stages can distinguish in the ANS's magmatic and tectonic evolution, which is produced due to various geodynamic events. These stages are: (i) The subduction stage was formed from the amalgamation of island-arc volcano-sedimentary sequences and plutonic rocks [2]–[5] (~870–670 Ma); (ii) continental collision stage (~650–640 Ma), included the formation of calc-alkaline gabbro's and granodiorites which, formed from the convergence between the juvenile accrete ANS crust with continental blocks of west Gondwana to form the East African orogen [6]–[9], and (iii) post-collisional stage (630-550 Ma), as defined by the calc-alkaline to alkaline/peralkaline volcanic and granitic rocks development [10]–[13].

According to [14], three main lithologic terrains make up Egypt's Eastern Desert (ED): i) the northern one, which is abundant in massive granites; ii) the central one, which has the greatest concentration of rocks with oceanic affinities; and iii) the southern one, which is abundant in gneissic granites. The Eastern Desert granitoid rocks of Egypt have been classified as syn- to late-orogenic granitoid assemblages (610-880Ma) and post-orogenic to anorogenic granitoids assemblages (475-600 Ma) [15]–[18]. The younger granites covered ≈ 22% of the total exposed Proterozoic belt, which fractionated to calc-alkaline I- and A-type granites such as alkali-feldspar granites, syenogranites, and monzogranites.

A-type granites are highly evolved and alkaline to peralkaline granites, and they have ages between 550 and 610 Ma based on the Rb-Sr and U-Pb age dating, respectively [19]–[21]. Rare metals bearing granitoids are volatile-rich rocks and highly evolved A-type granites, widespread in most Orogenic belts worldwide. They include granitoids that host the mineralization of one or more metal elements like U, Th, Nb, Ta, Sn, W, Zr and REEs. Moreover, they occasionally host rare metal minerals, such as uraninite, thorite, columbite, tantalite, pyrochlore, fergusonite, and cassiterite. Some of the Egyptian A-type granitoids host most of the known rare-metals (U, Th, W, Sn, Ta, Nb, Mo, and REE) such as Gabel Qattar (the subject of this study) and El-Erediya areas [22], [23]. Qattar younger granitoids classified as meta-aluminous

* Corresponding author at Zagazig University

E-mail addresses: omaramer@science.zu.edu.eg (Omar Amer)

mineralized A-type granites, which are affected by metasomatic alterations. Alterations lead to enrichment in the Y, W, U, Nb content and the chalcophile elements [24]–[29] in Qattar granitoids.

The significance of studying bulk geochemistry of granitoids and hosted fluorites from the Qattar pluton lies in its potential to provide valuable insights into mineral exploration and resource assessment. Major, trace, and rare-earth elements found in these geological materials can offer crucial information about the processes involved in their formation and their potential mineralization. By analyzing the bulk geochemistry, researchers can identify the source of the granitic rocks and evaluate their magmatic evolution, which can help determine the tectonic setting and the potential for associated mineral deposits. Moreover, studying trace and rare-earth elements can help identify geochemical anomalies and establish geochemical signatures associated with economically significant mineralization. Understanding the distribution and concentration of economically essential elements in granitoids and fluorites from the Qattar pluton can aid in targeting areas with high mineralization potential, guiding exploration efforts, and optimizing resource assessment strategies. The findings from these studies can contribute to informed decision-making in the mining industry, promoting efficient and sustainable resource extraction practices. The petrogenesis of A-type granitoids in ANS is still controversial, as various of their chemical characteristics do not reflect a proper crystal-melt balance. In this work, bulk geochemistry studies (major, trace, and rare-earth elements) of granitoids and hosted fluorites from Qattar pluton are presented, which investigate the origin and evolution of the post-collisional A-type Qattar granitic magmatism and its relevance to associated ore deposits.

2. Geological Background

The Qattar area, located in the Northeastern Desert of Egypt, exhibits a complex geological background shaped by various tectonic and magmatic events. The region comprises metamorphic and igneous rocks that provide valuable insights into the geological evolution of the area. The Qattar area is underlain by a basement complex composed of Precambrian rocks, including gneisses, schists, and granitic intrusions, indicating the presence of ancient crustal materials[25]. This basement complex has undergone multiple episodes of deformation and metamorphism, resulting in the formation of various structural features such as folds, faults, and shear zones. Also, this region is characterized by the presence of several granite plutons, including the Qattar pluton, which represents a significant magmatic event. These granitoid intrusions are commonly associated with tectonic processes such as subduction and collision, indicating the involvement of convergent plate boundaries in the geological history of the Qattar area. The emplacement of these granitoids has not only influenced the regional tectonic framework but has also contributed to the development of mineralization in the area.

Qattar granite intrusion covers around 35 km^2 between latitudes 27º 05` - 27º 07` N and longitudes 33º 14` 42`` - 33º 19` E (Fig. 1). These granites formed isolated masses of older diorite and granodiorite as well as rugged mountain peaks of pink to red medium-grained younger granites [25], [30], [31]. These granites are divided into the three phases G1, G2, and G3[25]. In addition to uranium mineralization, the younger granite has undergone several post-magmatic hydrothermal modifications, including fluoritization, hematitization, kaolinization, and epidotization [24]. Qattar granites are represented by syenogranites and alkali feldspar granites[22]. These granites comprise perthite, alkali-feldspar, quartz, plagioclase, biotite, and hornblende (found only in syenogranite). Magnetite, ilmenite, monazite, apatite, allanite, xenotime, and zircon are the main accessory minerals, whereas fluorite, muscovite, hematite, and clay minerals are found as secondary minerals[29], [32], [33].

The younger granite under study has undergone several post-magmatic hydrothermal alterations [24]. There are two types of mineralization in Gabal Qattar: 1) the U–fluorite and 2) molybdenum–bismuth–silver ores. The fluorite associated with U mineralization is exposed through mining works at more profound levels of granite [22]. Fluorite mineralization is hosted in alkali-feldspar granites, controlled by two conjugate fault systems trending NW–SE and NNE–SSW faults [34] (Fig. 1).The alkali-feldspar Qattar granite is medium to coarse-grained. These granitoids were composed of K-feldspars, quartz, plagioclase, and biotite. Fluorite, calcite, muscovite, magnetite, apatite, monazite and zircon found as minor and accessory minerals [22], [29].

3. Material and Methods

Twenty-four samples, representing 8 samples of Qattar granites and 16 of hosted fluorites, investigated in detail. The major, trace, and REE element concentrations (Tables 1 and 2) were carried out at the Earth Science Institute, Vienna University. The major and trace element concentrations were carried out by X-ray fluorescent (XRF) technique using a Philips PW 2400 series spectrometer on fused and pressed powder discs, respectively. Loss on ignition (LOI) was determined after igniting 5 g of rock sample powder in porcelain crucibles at 1050 °C for 1 H. Analytical precision is better than 1% and 2 - 5% for major and trace elements, respectively. REE concentrations were carried out with the inductively coupled plasma-mass spectrometer (ICP-MS) Elan 6100 with Hg Flow Injection System "FIMS 100" and Laser Sampler "LSX 200" has used for REE analyses.

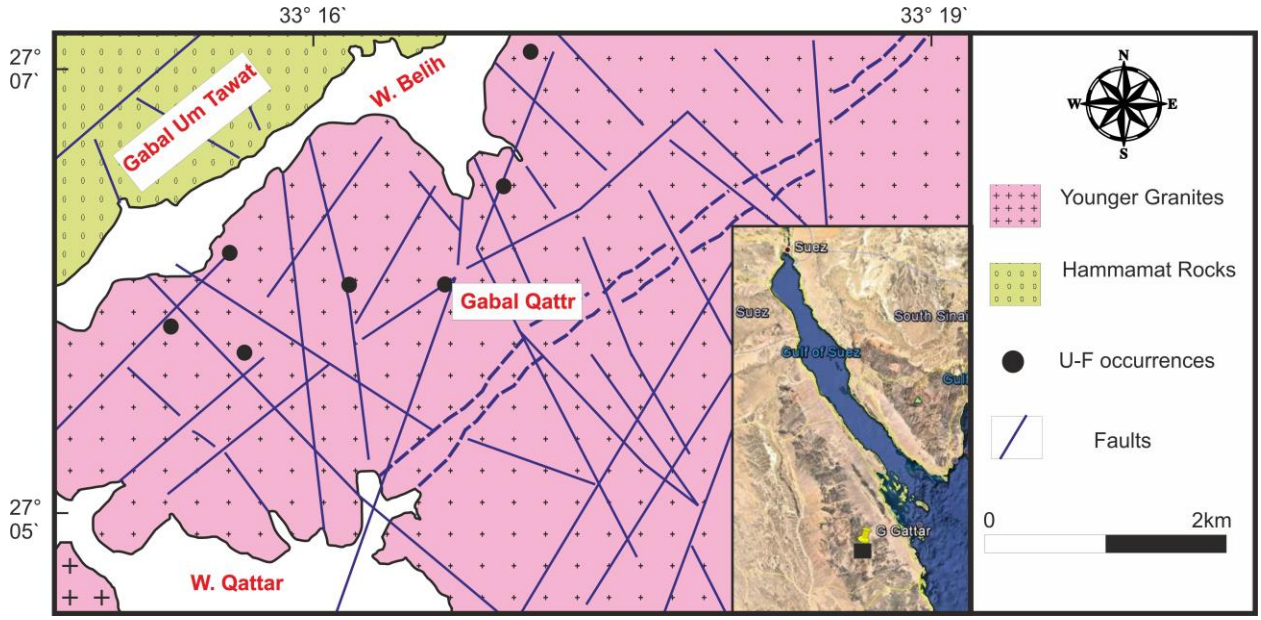

Fig. 1 Geological map of Qattar granite, North Eastern Desert, Egypt, modified after [22].

4. Result and discussion

4.1 Geochemical characteristics and tectonic setting

The major-, trace- and rare earth elements for Qattar granites listed in Table 1. These rocks are highly and limited variations of SiO_2 content ranging from 74.17 to 74.74 wt.% and have low abundances of Al_2O_3 (avg. 13.06 wt. %), MgO (avg. 0.03 wt. %), CaO (avg. 0.27 wt. %), Fe_2O_3 (avg. 0.92 wt. %), and high alkalis contents (Na_2O+K_2O=8.79–9.02 wt.%). Moreover, there are rich in high field-strength element contents (HFSE, Rb 341.33 ppm, Cs 14.6 ppm, Nb 156.9 ppm, Ta 10.14 ppm, Th 37.28 ppm, U 25.1 ppm, and Pb 18.13 ppm, on average; Table 1). All these features are characteristic of A-type granites [35], [36]. In the diagrams of ANNOR–Q'-F' and A/NK–A/CNK, the Qattar granites are plotted in the alkali-feldspar granite and peraluminous fields [37], [38] (Fig. 2a, b; respectively), reliable with their mineralogical characteristics. These rocks show high FeO^{tot}/ (FeO^{tot} +MgO=0.96–0.98) and are plotted in Ferron A-type granites (Fig. 2c) [39]. They investigated high K-calc-alkaline affinity with highly fractionated calc-alkaline (HFCA) rocks [40], [41] (Fig. 2d, e; respectively) and classified them as calc-alkaline Egyptian younger granitoids (Fig. 2f) [42]. Studied granites have K/Rb ratios (112.85-124.90) <140, which indicates the Rb separated during the aqueous liquid phase segregation stage at highly evolved melt [43], [44]. Moreover, they plotted enormously evolved and fractionated granitoids (Fig. 3a) [45] with barren nature [46] (Fig. 3b).

Qattar alkali feldspar granites have low total REE abundances (104.5–123.90 ppm), and display tetrad chondrite-normalized REE pattern [47] (Fig. 3c), characterized by slight enrichment in light REE (LREE; $(La/Yb)_N$ =0.32–0.61) with characteristic negative Eu anomalies (0.10–0.28). They display insignificant fractionations LREE $(La/Sm)_N$ =0.61-1.57) and (high REE) HREE $(Gd/Yb)_N$= 0.45-0.50), accepted with those of the calc-alkaline granitoids of Sinai [12], indicating these rocks have resulted from volatiles transfer of REEs by F complexes [48]. The primitive mantel-normalized diagram [47] (Fig. 3d) exhibits negative Sr, P, and Ti anomalies and weak to moderate La, Ba, Ce, Pr, P, Eu, and Yb anomalies, which indicate plagioclase, K-feldspar, titanate, and apatite fractionated in that order of the magma. Moreover, Ti, Nb, P, and Sr depletion indicate granite derivation from crustal protolith [49]. Qattar granites have high 10,000×Ga/Al ratios (6.04 to 6.42), higher than the S- and I-type granites (avg. 2.28 and 2.1028, respectively; [36]. Moreover, they fall in the A-type granite fields (Fig. 3e, f) [36] and fall in the fraction crystallization granites (A1 subtype; Fig. 4a) [50].

4.2 Crystallization Signatures

By using the Al-Ti thermometer [51], Qattar granitoids show high emplacement temperature (avg. 755.3 °C), which indicates highly fractionated granites [52]. The crystallization pressures were determined by using the equation proposed by [53]:

$$P= -980.74\times(Qz) + 26.392\times(Qz)^2-0.2426 \times (Qz)^3 + 12563 \quad (1)$$

Where (P) is the determined pressure and (Qz) is normative quartz value.

Applying of this equation indicates that Qattar granites crystallized under pressures ranging from 2.33 to 2.95 kbars. Moreover, the emplacement depth could calculate using the equation of [53] depending on the estimated pressures and density of continental crust (2.85 g/cm3), equivalent to 8.33-10.57-km depth.

The Oxygen fugacity buffers (log fO_2) can be calculated by using [54] equilibrium expression:

Log (fO_2) = 9.36 - [24930 / T (k)] + 0.046[(P (kb)-1/T (k)] (2)

Where (P) is the pressure in kbar and (T) is the temperature in K

The occurrence of magnetite minerals compared to Fe-Ti oxides [33] in Qattar granitoid support their crystallization under oxidizing conditions and controlled by NNO fugacity buffer (log fO_2 from -14.91 to -14.85, Fig. 4b) [55].

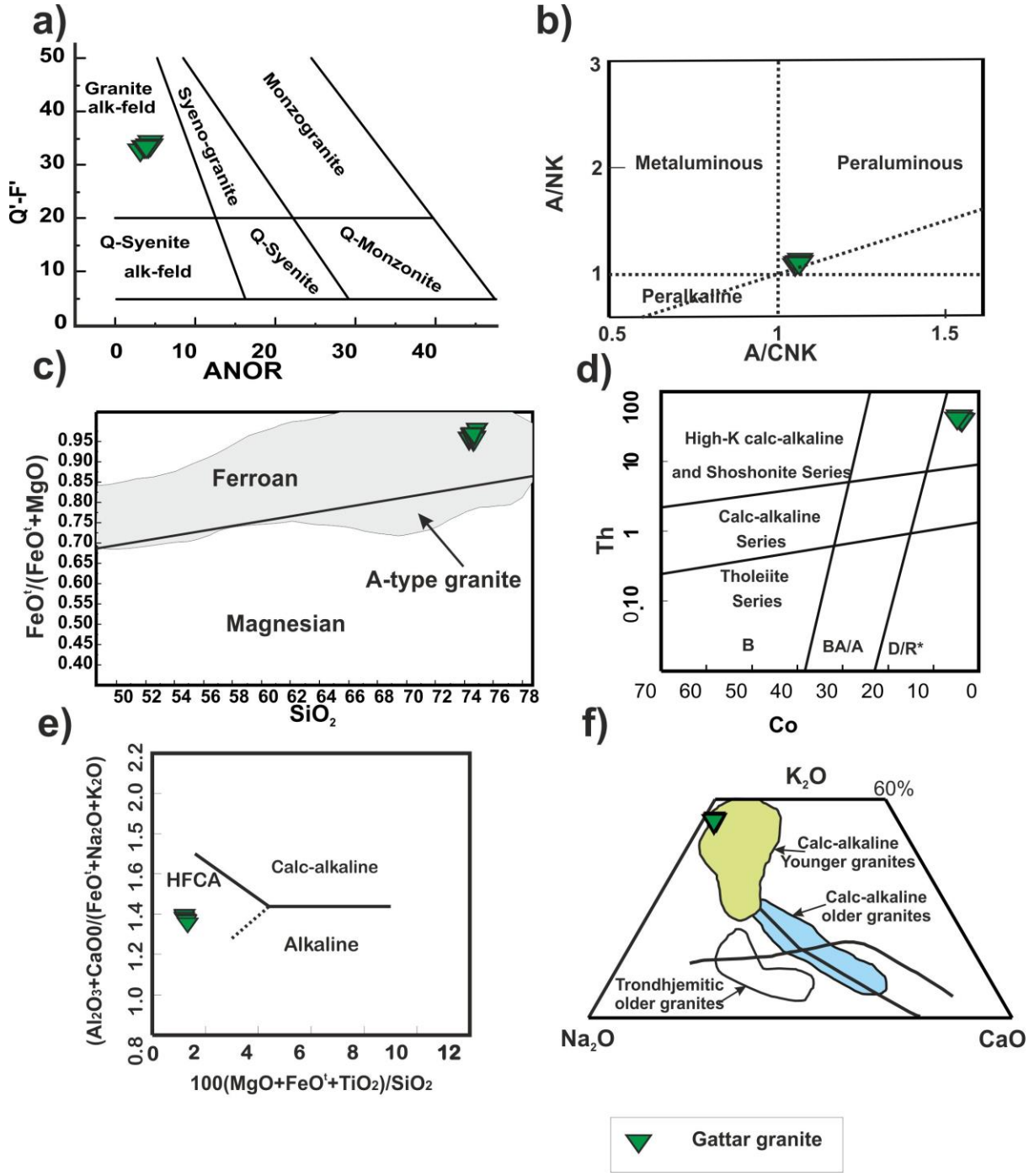

Fig. 2 (a) Q´- F´-ANOR diagram [38]; (**b)** Al_2O_3/CaO+Na_2O+K_2O - Al_2O_3/Na_2O+K_2O diagram[37]; **(c))** SiO_2-FeO^{tot}/FeO^{tot}+ MgO after [39]; **(d)** Co-Th variation diagram after [40]; **(e)** Al_2O_3+Cao/FeO^{tot}+Na_2O+K_2O-100*(TiO_2+FeO^{tot}+MgO)/SiO_2 variation diagram [41]; **(f)** Na_2O-CaO-K_2O ternary diagram showing the Egyptian younger and older granitoids fields after [42].

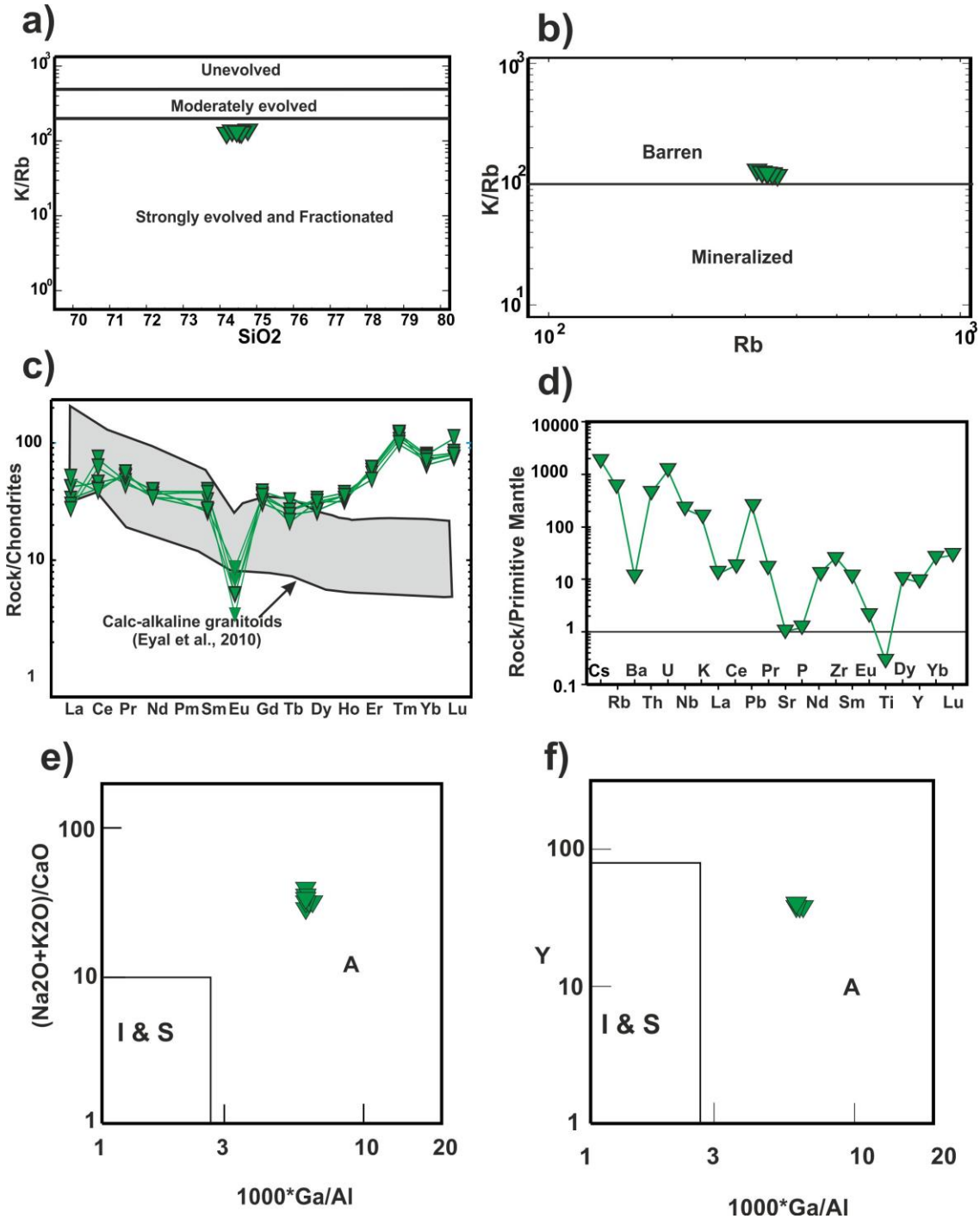

Fig. 3 (a) Blevin's K/Rb−SiO_2 diagram[45]; **(b)** Variations of K/Rb - Rb ratios of the studied granites [46]; **(c)** REE chondrite-normalized diagram [47] of Qattar granitoids. **(d)** Primitive mantle -normalized diagram [47] of Qattar granitoids; **(e; f)** Na_2O+K_2O- 10,000 Ga/Al, and FeO^{tot}/MgO-Zr+Nb+Ce+Y diagrams for A type granites [36].

4.3 Fluorine-uranium (F-U) contents and REEs Tetrad Effect

The highly differentiated Qattar granitoids exhibit an M-type tetrad effect (Fig. 3c), which is comparable to the REEs tetrad effects produced in the highly F-rich differentiated granites from the El-Erediya pluton in Egypt and Qianlishan composite plutons, S. China [23], [56], respectively). In characteristic magmatic systems, CHARAC (CHArge- and RAdius-Controlled) trace-element behaviors predominated, but the lanthanides tetrad effects were commonly associated with non-CHARAC trace-element behaviors. Y-Ho, Zr-Hf, etc. pairs (elements with similar charge and radius) were controlled by chemical integration processes that led to trace element fractionations characterized by a geochemical system of non-CHARAC behavior [57], [58]. The Qattar granites show non-CHARAC behavior [57] (Fig. 4c). Besides, it occurs in highly evolved magmatic systems (rich in CO_2, H_2O, B, Li,

F, and/or Cl), which may be developed between hydrothermal fluids and pure silicate-melts in late-stage of crystallization [57], [59]. The REEs tetrad effect and non-CHARAC trace element behavior of Qattar granitoids are often related to F-rich granitic magmas [58], [60], [61].

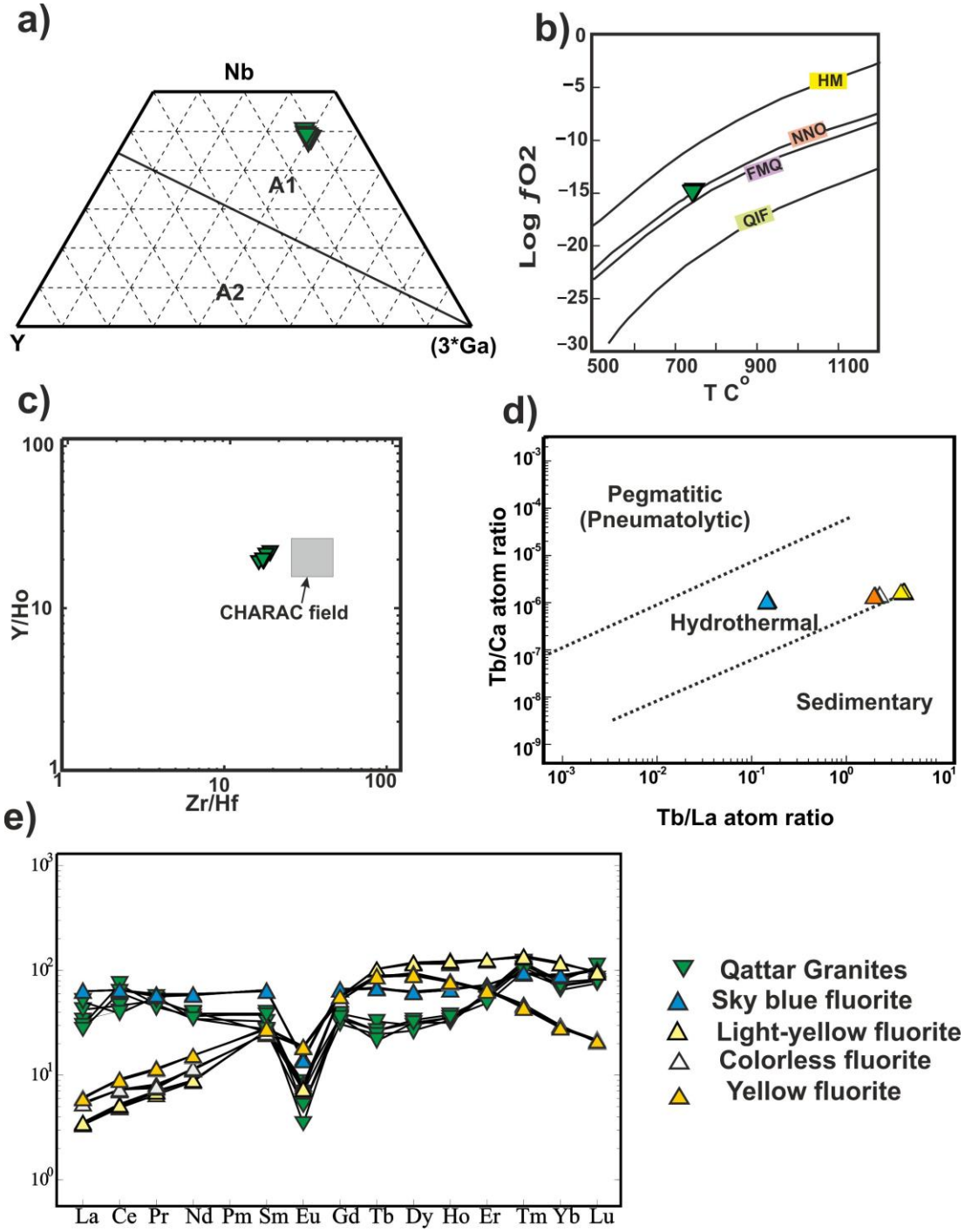

Fig. 4 (a) Nb-Y-3*Ga triangular diagram of[50]; **(b)** Temperature-oxygen fugacity (fO_2) diagram [55]; **(c)** Y/Ho-Zr/Hf diagram with (CHARAC) field after[57] ; **(d)** Tb/Ca-Tb/La variation ratios of Qattar fluorites[69]; **(e)** REE chondrite-normalized patterns of Qattar granite and their hosted fluorite [47].

Table 1. Major, trace and REE of the granites at Qattar area.

	QGr 1	QGr2	QGr 3	QGr 4	QGr 5	QGr 6	QGr 7	QGr 8	Average (avg.)
Major oxides (Wt %)									
SiO_2	74.74	74.52	74.17	74.33	74.57	74.53	74.58	74.45	74.49
$Al2O_3$	12.88	13.1	13.23	13.13	12.98	13.03	13.1	13.05	13.06
Fe_2O_3	0.94	0.89	0.92	0.87	0.99	0.9	0.93	0.93	0.92
MgO	0.02	0.04	0.04	0.03	0.04	0.03	0.04	0.03	0.034
CaO	0.3	0.27	0.23	0.28	0.25	0.28	0.25	0.26	0.27
Na_2O	3.95	4.02	4.11	4.06	4	4.01	4.04	4.03	4.028
K_2O	4.84	4.8	4.91	4.81	4.94	4.81	4.88	4.87	4.86
TiO_2	0.06	0.06	0.06	0.06	0.06	0.06	0.06	0.06	0.06
P_2O_5	0.03	0.02	0.03	0.03	0.03	0.02	0.02	0.03	0.03
MnO	0.15	0.15	0.13	0.14	0.14	0.15	0.14	0.14	0.14
F	0.08	0.09	0.1	0.09	0.09	0.08	0.09	0.09	0.09
LOI	1.62	1.58	1.68	1.68	1.62	1.62	1.62	1.65	1.63
total	99.57	99.51	99.58	99.47	99.68	99.52	99.75	99.58	99.58
Trace elements (ppm)									
Ba	75	78.5	81	73.5	82.5	75.7	80.7	78	78.11
Be	18.5	15.5	14.5	17	16	17	15.3	16.5	16.29
Co	3.7	3.9	3.7	3.8	3.7	3.8	3.7	3.7	3.75
Cs	14.7	14.6	14.5	14.5	14.7	14.6	14.6	14.6	14.6
Ga	41.5	44.5	42.5	42	42	42.7	43	42	42.52
Hf	16.4	16.2	16.3	16.5	16.2	16.3	16.2	16.3	16.3
Nb	163.7	157.7	149.7	154.2	159.2	158.5	155.5	156.7	156.9
Rb	321.7	340.9	361.2	331.4	351.5	331.3	351.2	341.4	341.33
Sn	8.5	9	8.5	8.5	8.5	8.7	8.7	8.5	8.61
Sr	21.7	22.2	21.5	21.7	21.5	21.8	21.7	21.6	21.71
Ta	10	10.3	10.2	10.1	10.1	10.1	10.2	10.1	10.14
V	8	7.5	7.5	7.5	8	7.7	7.7	7.8	7.71
W	51.7	48.7	42.4	47.1	47	49.1	46	47	47.38
Zr	316	285.5	266	301.5	280.5	301	277.3	291	289.85
Y	38.7	38	39.5	39.4	38.8	38.7	38.7	39.1	38.86
Mo	6.1	6.7	6.4	6.1	6.3	6.3	6.4	6.2	6.31
Cu	5.5	5.6	5.5	5.5	5.6	5.5	5.5	5.5	5.53
Pb	18	18.1	18.3	18.1	18.2	18	18.2	18.1	18.13
Zn	221.5	218	221.5	228.5	214.5	222.7	218	221.5	220.78
Ni	3.1	2.9	2.9	3.1	2.9	3	2.9	3	2.98
As	0.8	0.8	0.8	0.8	0.8	0.8	0.8	0.8	0.8

Cd	0.1	0.1	0.1	0.1	0.1	0.1	0.1	0.1	0.1
Sb	0.1	0.1	0.1	0.1	0.1	0.1	0.1	0.1	0.1
Bi	7.3	7.7	7.7	7.1	7.9	7.3	7.7	7.5	7.525
Ag	0.1	0.1	0.1	0.1	0.1	0.1	0.1	0.1	0.1
U	22.5	25.5	27.5	24	26	24	26.3	25	25.1
Th	36.3	34	40	36.3	40	35.5	38	38.1	37.28
K/Rb	124.9	116.9	112.85	120.5	116.68	120.53	115.36	118.43	118.27
Na_2O+K_2O	8.79	8.82	9.02	8.87	8.94	8.82	8.92	8.9	8.89
$FeO^{tot}/FeO^{tot}+MgO$	0.98	0.96	0.96	0.97	0.96	0.97	0.96	0.97	0.97
10000*Ga/Al	6.09	6.42	6.07	6.04	6.11	6.19	6.20	6.08	6.15
REEs (ppm)									
La	8	7	6.50	10.00	12.00				8.7
Ce	25	45	38.00	28.00	24.00				32
Pr	5	4.5	4.20	4.90	5.30				4.78
Nd	18	16	17.00	18.50	16.00				17.1
Sm	6	5	5.80	4.00	4.20				5
Eu	0.3	0.2	0.40	0.30	0.50				0.34
Gd	7.5	8	7.00	6.40	7.20				7.22
∑LREEs	69.8	85.7	78.9	72.1	69.2				75.14
Tb	1	1.2	1.00	0.90	0.80				0.98
Dy	8	7.5	8.50	6.70	8.00				7.74
Ho	1.8	2	2.10	1.90	2.00				1.96
Er	10	9.5	9.00	10.20	8.00				9.34
Tm	3	2.9	2.70	3.10	2.50				2.84
Yb	13.5	13	12.50	11.00	12.00				12.4
Lu	2.8	2.1	2.00	1.90	2.00				2.16
∑LREEs	40.1	38.2	37.8	35.7	35.3				37.42
∑REEs	109.90	123.90	116.70	107.8	104.5				112.56
Some geochemical ratios									
Eu/Eu*	0.14	0.10	0.19	0.18	0.28				0.18
$(La/Sm)_N$	0.73	0.77	0.61	1.37	1.57				1.01
$(La/Yb)_N$	0.36	0.33	0.32	0.55	0.61				0.43
$(Gd / Yb)_N$	0.45	0.5	0.45	0.47	0.49				0.47
T_Al/Ti.exp.C	756.6	754.9	753.90	754.7	755.8	755.4	754.9		755.30
log ƒO_2-	-14.85	-14.89	-14.91	-14.89	-14.87	-14.88	-14.89		-14.88
P	2.33	2.49	2.95	2.65	2.60	2.48	2.60		2.61
Depth	8.33	8.90	10.57	9.49	9.29	8.87	9.32		9.35

*The normalization is based on the chondrite-normalized data given by [47] (1989): Eu anomaly is defined by $Eu/Eu^* = Eu_N /(\sqrt{Sm_N \chi Gd_N})$.

Qattar granites considered as uraniferous granites (U avg. 25.1 ppm > 4 ppm Clark value 4 ppm). Most U is found in high-temperature magma-hydrothermal systems as a compound with F [62]. F tends to change the liquidus phase and is also suited to produce melt depolymerization, which increases the solubility of U in the magma [63], [64]. The U fluid-magma partition coefficients are extremely low, ranging from 0.03 to 0.04 [65]. As a result, F-rich-magma tends to have a higher U concentration [66]. Besides, Qattar alkali-feldspar granites contain insignificant amounts of biotite and apatite minerals, which F in magma tends to join in its crystal lattices in the post-magmatic stages [31], [67]. So, these granites are considered as highly evolved F-enriched granites [33]. Additionally, according to [68] F and U are two elements accumulating in residual melts during crystal differentiation. In oxidizing conditions, F can change the valency of uranium from U^{4+} to U^{6+} and produce soluble fluoride or hydroxyfluoride complexes as the U-F combination.

4.4 Geochemistry of Fluorite

Qattar fluorites are classified into four types (sky blue-, light-yellow-, colorless- and yellow-type), according to the mineral chemistry analysis (Table 2). From the Tb/Ca-Tb/La diagram [69], these fluorites were formed by hydrothermal processes (Fig. 4d). The colorless fluorite is abundant in trace elements, particularly Ti, Ba, Pb, Sr, and Zn (Table 2). The trace element enrichments in these fluorite-bearing granites compared to barren fresh granites (Fig. 3b) are suitable for leaching from major and accessory minerals of Qattar granite during fluid-mineral interactions [22].

Table 2: Chemical analyses of the Qattar fluorites

	F01	F01a	F01b	F01d	**Avg.**	**F02**	F02b	F02c	F02e	**Avg.**
	sky blue fluorites					**Light-yellow fluorites**				
Ca wt %	56.71	58.42	57.96	56.35	**57.36**	56.69	56.85	57.91	55.49	**56.74**
Na	0.11	0.11	0.11	0.11	**0.11**	0.17	0.17	0.17	0.17	**0.17**
	0.004	0.004	0.004	0.004	**0.004**	0.02	0.02	0.02	0.02	**0.02**
Mg	0.005	0.004	0.005	0.004	**0.004**	0.02	0.02	0.02	0.02	**0.02**
Fe	0.25	0.24	0.24	0.24	**0.24**	0.27	0.27	0.27	0.27	**0.27**
Al	0.02	0.02	0.02	0.02	**0.02**	0.03	0.03	0.03	0.03	**0.03**
Mn	0.01	0.01	0.01	0.01	**0.01**	0.01	0.01	0.01	0.01	**0.01**
Ti	0.04	0.04	0.04	0.04	**0.04**	0.05	0.05	0.05	0.05	**0.05**
F	42.12	40.29	41.06	42.12	**41.40**	41.25	42.36	40.28	43.21	**41.78**
SI	0.01	0.02	0.01	0.11	**0.04**	0.09	0.08	0.07	0.10	**0.09**
total	99.28	99.17	99.47	99.02	**99.23**	98.61	99.87	98.84	99.38	**99.17**
	Trace elements and REE (ppm)									
Ba	2.50	2.60	2.55	2.58	**2.56**	4.00	4.20	4.10	4.15	**4.11**
Co	0.78	0.77	0.78	0.77	**0.77**	0.95	1.00	0.98	0.99	**0.98**
Cr	6.50	6.30	6.40	6.35	**6.39**	4.80	4.60	4.70	4.65	**4.69**
Cu	13.60	12.90	13.25	13.08	**13.21**	98.40	98.20	98.30	98.25	**98.29**
Li	2.67	2.59	2.63	2.61	**2.63**	0.34	0.31	0.33	0.32	**0.32**
Mo	15.27	15.23	15.25	15.24	**15.25**	0.40	0.35	0.38	0.36	**0.37**
Ni	1.50	1.30	1.40	1.35	**1.39**	11.70	12.10	11.90	12.00	**11.93**
Pb	43.10	42.20	42.65	42.43	**42.59**	6.00	5.80	5.90	5.85	**5.89**
Rb	0.12	0.10	0.11	0.11	**0.11**	0.37	0.32	0.35	0.33	**0.34**
Sr	33.70	33.10	33.40	33.25	**33.36**	15.70	15.20	15.45	15.33	**15.42**
Zn	34.20	35.00	34.60	34.80	**34.65**	61.50	62.50	62.00	62.25	**62.06**
Sb	0.13	0.10	0.12	0.11	**0.11**	0.21	0.20	0.21	0.20	**0.20**
V	0.90	0.90	0.80	0.85	**0.86**	0.80	1.00	1.00	1.00	**0.95**

Sc	0.50	0.60	0.50	0.55	**0.54**	0.50	0.60	0.50	0.55	**0.54**
Y	308.85	307.54	308.20	307.87	**308.11**	682.35	683.21	682.78	683.00	**682.83**
La	15.07	15.12	15.10	15.11	**15.10**	0.79	0.84	0.82	0.83	**0.82**
Ce	39.23	39.85	39.54	39.70	**39.58**	3.01	3.21	3.11	3.16	**3.12**
Pr	5.70	5.40	5.55	5.48	**5.53**	0.62	0.68	0.65	0.67	**0.65**
Nd	27.75	27.26	27.51	27.38	**27.47**	4.10	4.21	4.16	4.18	**4.16**
Sm	9.77	9.85	9.81	9.83	**9.82**	4.02	4.09	4.06	4.07	**4.06**
Eu	0.84	0.79	0.82	0.80	**0.81**	0.48	0.41	0.45	0.43	**0.44**
Gd	13.32	13.54	13.43	13.49	**13.44**	11.56	11.62	11.59	11.61	**11.59**
∑LREE	111.68	111.81	111.75	111.78	**111.75**	24.58	25.06	24.82	24.94	**24.85**
Tb	2.57	2.49	2.53	2.51	**2.53**	3.81	3.84	3.83	3.83	**3.83**
Dy	15.58	15.96	15.77	15.87	**15.79**	29.64	30.00	29.82	29.91	**29.84**
Ho	3.68	3.74	3.71	3.73	**3.71**	6.57	7.00	6.79	6.89	**6.81**
Er	12.13	12.02	12.08	12.05	**12.07**	20.56	21.00	20.78	20.89	**20.81**
Tm	2.33	2.41	2.37	2.39	**2.38**	3.36	3.48	3.42	3.45	**3.43**
Yb	14.93	15.10	15.02	15.06	**15.03**	19.76	20.00	19.88	19.94	**19.90**
Lu	2.53	2.62	2.58	2.60	**2.58**	2.46	2.41	2.44	2.42	**2.43**
∑HREE	53.75	54.34	54.05	54.19	**54.08**	86.16	87.73	86.95	87.34	**87.04**
REE	165.43	166.15	165.79	165.97	**165.84**	110.74	112.79	111.77	112.28	**111.89**
Th	1.10	1.00	0.90	0.95	**0.99**	0.40	0.50	0.40	0.45	**0.44**
U	1.30	1.40	1.35	1.38	**1.36**	0.80	0.70	0.75	0.73	**0.74**
Gd / Yb norm	0.72	0.73	0.72	0.72	**0.72**	0.47	0.47	0.47	0.47	**0.47**
Eu/Eu*	2.61	2.60	2.61	2.60	**2.60**	1.80	1.81	1.80	1.81	**1.80**
	F03	F03c	F03d	F03f	**Avg.**	F04	F04d	F04e	F04g	**Avg.**
	Colorless fluorites					**Yellow fluorites**				
Ca wt %	55.47	57.01	57.48	57.12	**56.77**	58.95	58.94	56.63	58.41	**58.23**
Na	0.13	0.13	0.13	0.13	**0.13**	0.14	0.14	0.14	0.14	**0.14**
K	0.00	0.00	0.00	0.00	**0.00**	0.00	0.00	0.00	0.00	**0.00**
Mg	0.01	0.01	0.01	0.01	**0.01**	0.01	0.01	0.01	0.01	**0.01**
Fe	0.26	0.26	0.26	0.26	**0.26**	0.25	0.25	0.25	0.25	**0.25**
Al	0.02	0.02	0.02	0.02	**0.02**	0.01	0.01	0.01	0.01	**0.01**
Mn	0.01	0.01	0.01	0.01	**0.01**	0.01	0.01	0.01	0.01	**0.01**
Ti	0.04	0.04	0.04	0.04	**0.04**	0.04	0.04	0.04	0.04	**0.04**
F	43.02	41.23	41.53	41.36	**41.79**	39.86	40.22	42.32	40.28	**40.67**
Sl	0.12	0.14	0.05	0.17	**0.12**	0.07	0.05	0.12	0.18	**0.11**
total	99.08	98.85	99.53	99.12	**99.14**	99.34	99.67	99.53	99.33	**99.47**
Trace elements and REE (ppm)										
Ba	132.80	134.00	133.40	133.70	**133.48**	1.90	2.00	1.95	1.98	**1.96**
Co	0.80	0.75	0.78	0.76	**0.77**	0.85	0.82	0.84	0.83	**0.83**
Cr	9.80	9.50	9.65	9.58	**9.63**	9.60	9.60	9.60	9.60	**9.60**

Cu	32.10	32.20	32.15	32.18	**32.16**	14.60	14.40	14.50	14.45	**14.49**
Li	0.33	0.34	0.34	0.34	**0.34**	0.14	0.13	0.14	0.13	**0.13**
Mo	0.45	0.42	0.44	0.43	**0.43**	21.62	21.74	21.68	21.71	**21.69**
Ni	11.10	11.30	11.20	11.25	**11.21**	11.40	11.54	11.47	11.51	**11.48**
Pb	643.80	649.50	646.65	648.08	**647.01**	54.80	55.00	54.90	54.95	**54.91**
Rb	0.15	0.16	0.16	0.16	**0.16**	0.10	0.10	0.10	0.10	**0.10**
Sr	116.00	112.00	114.00	113.00	**113.75**	40.50	41.20	40.85	41.03	**40.89**
Zn	55.20	54.80	55.00	54.90	**54.98**	52.70	53.20	52.95	53.08	**52.98**
Sb	0.01	0.01	0.01	0.01	**0.01**	0.02	0.02	0.02	0.02	**0.02**
V	0.90	0.90	0.70	0.80	**0.83**	0.80	0.70	0.70	0.70	**0.73**
Sc	0.50	0.70	0.60	0.65	**0.61**	0.50	0.50	0.50	0.50	**0.50**
Y	302.36	301.54	301.95	301.75	**301.90**	352.82	353.24	353.03	353.14	**353.06**
La	1.27	1.28	1.28	1.28	**1.28**	1.46	1.41	1.44	1.42	**1.43**
Ce	4.49	4.42	4.46	4.44	**4.45**	5.50	5.58	5.54	5.56	**5.55**
Pr	0.78	0.71	0.75	0.73	**0.74**	1.07	1.11	1.09	1.10	**1.09**
Nd	5.23	5.42	5.33	5.37	**5.34**	7.12	7.14	7.13	7.14	**7.13**
Sm	3.79	3.82	3.81	3.81	**3.81**	4.27	4.25	4.26	4.26	**4.26**
Eu	1.07	1.09	1.08	1.09	**1.08**	1.06	1.09	1.08	1.08	**1.08**
Gd	10.71	10.74	10.73	10.73	**10.73**	11.47	11.51	11.49	11.50	**11.49**
∑LREE	27.34	27.48	27.41	27.45	**27.42**	31.95	32.09	32.02	32.06	**32.03**
Tb	3.24	3.26	3.25	3.26	**3.25**	3.25	3.29	3.27	3.28	**3.27**
Dy	23.52	23.64	23.58	23.61	**23.59**	22.89	23.00	22.95	22.97	**22.95**
Ho	4.52	4.48	4.50	4.49	**4.50**	4.37	4.32	4.35	4.33	**4.34**
Er	10.81	10.88	10.85	10.86	**10.85**	10.59	10.62	10.61	10.61	**10.61**
Tm	1.18	1.21	1.20	1.20	**1.20**	1.14	1.11	1.13	1.12	**1.12**
Yb	4.90	5.10	5.00	5.05	**5.01**	4.87	4.82	4.85	4.83	**4.84**
Lu	0.54	0.52	0.53	0.53	**0.53**	0.56	0.53	0.55	0.54	**0.54**
∑HREE	48.71	49.09	48.90	49.00	**48.92**	47.67	47.69	47.68	47.69	**47.68**
REE	76.05	76.57	76.31	76.44	**76.34**	79.62	79.78	79.70	79.74	**79.71**
Th	0.30	0.20	0.10	0.15	**0.19**	0.80	0.70	0.80	0.75	**0.76**
U	1.00	0.80	0.80	0.80	**0.85**	1.00	0.50	0.70	0.60	**0.70**
$(Gd / Yb)_N$	1.77	1.70	1.74	1.72	**1.73**	1.91	1.93	1.92	1.93	**1.92**
Eu/Eu*	1.81	1.82	1.82	1.82	**1.82**	1.86	1.85	1.86	1.85	**1.86**

REE of Qattar fluorites (Table 2) shows a wide variety of variation (∑REE from 76.05 to 166.15) according to the variability of the parameters during the mineralization process [70]. The total REE in the sky-blue and light-yellow fluorites (avg. ∑REE 165.84 and 111.89, respectively) are higher than the colorless and yellow fluorites (avg. ∑REE 76.34 and 79.71, respectively) (Table 2). Figure 4e shows the chondrite-normalized REE patterns of Qattar granites and the hosted fluorite exhibiting a negative Eu anomaly (1.81-2.60; Tables 2, 3), indicating the crystallization temperatures above 200 °C [71]–[74]. The Eu anomaly is controlled by thermal, chemical, and redox conditions at average temperatures < 200 °C [26]. Moreover, sky blue and light-yellow fluorites exhibit higher values of LREE compared to HREE and (Gd / Yb) ratios < 1, in contrast with colorless and yellow fluorite show higher values of HREE compared to LREE and (Gd / Yb) ratios >1. These different fluorite patterns denoted that: 1) strong effects of

chemical interaction and physiochemical conditions of REE leaching [74] and 2) the parent fluids interacted with host rocks under reduced or weakly oxidizing conditions, backed found amount of sulfides in Qattar granite [22], [26], [73], [75].

4.5 Petrogenesis

The Qattar highly differentiated granites had numerous A-type granite features, including 1) high SiO_2, Na_2O+K_2O, Zr, Nb, and Rb; 2) high 10000*Ga/Al ratio (avg. 6.15); 3) high K-calc-alkaline natures and weakly peraluminous; 4) MgO, P_2O_5, TiO_2, CaO, Eu, and Sr contents depletion [35], [36], [76], [77]. On the other hand, the low Eu/Eu* ratio (avg. 0.18) showed that the Qattar A-type granites are highly differentiated [57]. Comparing these ratios with the lithospheric root propose contributions of slab break-off and/or lower crust [78], [79] at depth > 30km (Fig. 5a) [80]. U and Th have negative correlations with Zr/U and Zr/Th ratios (Fig. 5b, c; respectively), indicating that U-Th elements are controlled by Qattar granitoids magmatic accessory minerals [29]. However, the U and Th contents showed that magmatic fractionation was applied to the Qattar melt, which affects magmatic and late- to post-magmatic processes related to the exsolution of a fluid phase (Fig. 5d) [81]. Moreover, in the H_2O-F haplogranite Qz-Ab-Or- system (Fig. 5e) Qattar granitoids were plotted close to the minimum melt composition in the existence of fluorine at temperature ≈ 780 °C and pressure 2-5 kbar [82]–[84]. Moreover, Qattar granites are post-collisional tectonic settings (Fig. 5f) [37], supported by [85].

4.6 Geodynamic implications

The origin of post-collision magmatism in the ANS can be used to explain the extensional collapse, followed by continental collision from 600 to 650 Ma between West Gondwana and the juvenile ANS crust [86] (Fig. 6a). According to many studies [4], [8]–[10], [87], this continental collision affected significant crustal thickening, but the extensional collapse formed at 550 to 600Ma and caused the thicker lithosphere to weaken (Fig. 6b, c). The extensional collapse was regulated by lithospheric delamination and slab break-off [10], [12], [88], [89]. During the late collisional stage (630–610 Ma), a slab window opened, and unusually elevated temperatures supplied by the upwelling asthenosphere (Fig. 6 b, c), which caused an extensive melting process [90], (Fig. 6d). At late-collisional to early post-orogenic (610–280 Ma) stages, calc-alkaline and alkaline magmas were obtained in the ANS [12], [91], which included rich K calc-alkaline Qattar granitoids.

5. The study contribution to Sustainable Development Goals (SDGs)

Studying the bulk geochemistry of granitoids and hosted fluorites from the Qattar pluton aligns with several Sustainable Development Goals (SDGs), promoting sustainable economic development and responsible resource management.

This research contributes to SDG 9: Industry, Innovation, and Infrastructure, by providing valuable scientific knowledge that can support the development of sustainable mining practices. By understanding the geochemical characteristics of these geological materials, mining companies can optimize their exploration efforts, reducing the environmental impact associated with mineral extraction and ensuring efficient resource use. Furthermore, this research also supports SDG 12: Responsible Consumption and Production. By studying the bulk geochemistry of granitoids and fluorites, it becomes possible to identify areas with high mineralization potential, leading to targeted mining activities and minimizing waste generation. This knowledge can help promote the sustainable production of mineral resources, reducing the environmental footprint and ensuring the responsible use of natural resources. Moreover, SDG 13: Climate Action can be linked to this research through its potential to inform sustainable resource management strategies. Understanding the geological processes and mineralization associated with granitoids and fluorites can aid in identifying mineral deposits, including those relevant to renewable energy technologies. Directing exploration efforts towards these resources supports the transition to a low-carbon economy and contributes to mitigating climate change.

Therefore, the scientific studies on the bulk geochemistry of granitoids and hosted fluorites from the Qattar pluton have the potential to positively impact multiple SDGs, promoting sustainable economic development, responsible resource extraction, and climate action.

6. Future directions

Several future recommendations and areas for further study can be proposed to advance the understanding of the bulk geochemistry of granitoids and hosted fluorites from the Qattar pluton.

Petrogenetic Modeling: Petrogenetic modeling techniques, such as geochemical modeling and thermodynamic calculations, can help reconstruct the magmatic history and source characteristics of the granitoids. These models can provide insights into the melting processes, magma evolution, and magma source regions, aiding in interpreting the geochemical signatures observed in the rocks[56] .

Integration with geophysical surveys, remote sensing, and machine learning: Integrating bulk geochemical data with these techniques can facilitate the correlation between geochemical anomalies and subsurface structures or mineralization zones. This multidisciplinary approach can enhance the understanding of the spatial distribution of mineralization and assist in target selection for future exploration efforts [92], [93].

Environmental Implications: Investigating the potential environmental implications of the granitoids and hosted fluorites, especially regarding the presence of trace elements and rare-earth elements, is crucial. Assessing the mobility and behavior of these environmental elements can provide insights into potential environmental risks associated with mining activities and aid in developing sustainable mining practices.

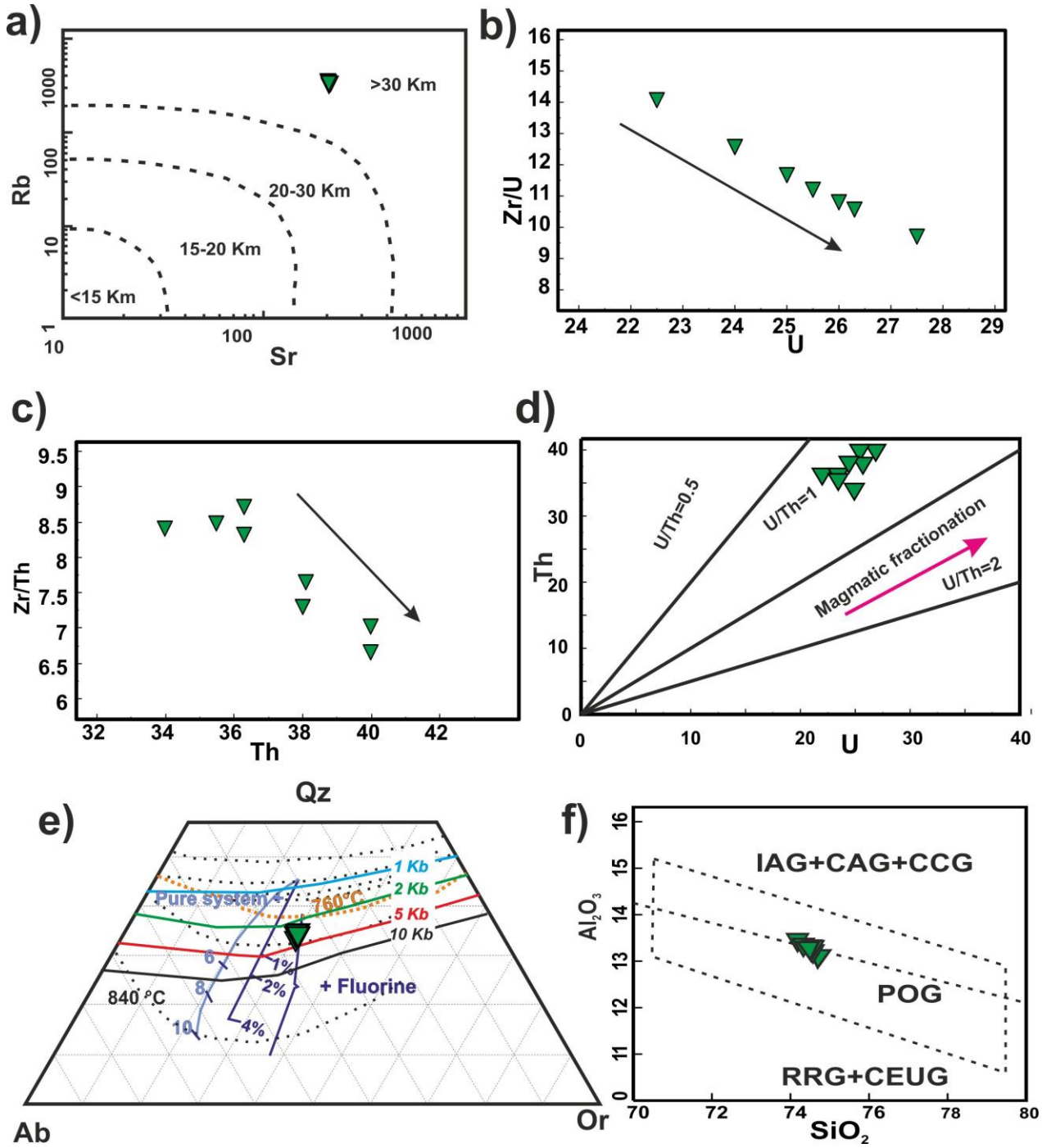

Fig. 5 (a) Sr-Rb diagram[80]; **(b; c; d)** U-Zr/U; Th- Zr/Th; U-Th for Qattar granitoids; **(e)** Qz-Ab-Or ternary diagram, temperature lines proposed by [82], pressure lines proposed by [84] and fluorine content proposed by [83]**; (f)** SiO_2 -Al_2O_3 variation diagram [37].

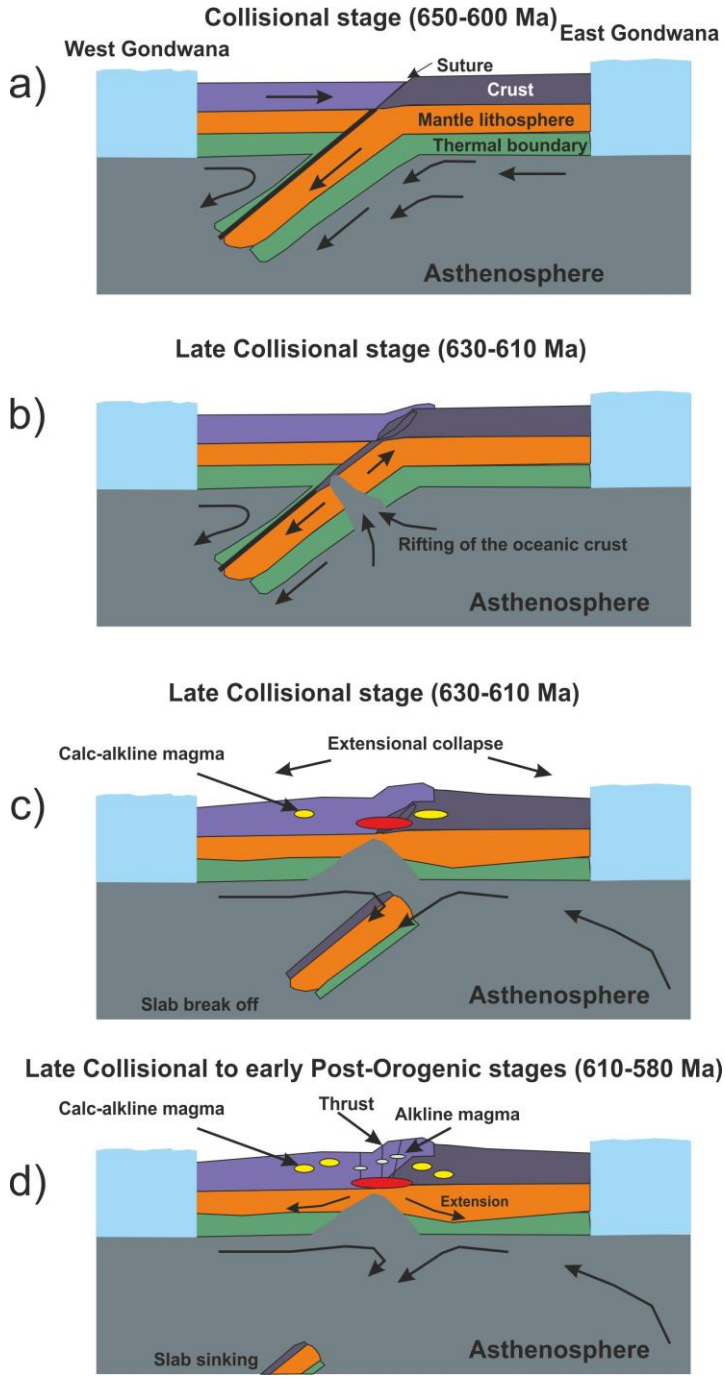

Fig. 6 Schematic tectono–magmatic evolution of the post-collisional stage of younger granite of Qattar area in the ANS (modified after;[10], [18], [87], [88], [91] **(a)** The start of collision between East and West Gondwana, (650–600Ma); **(b)** Starting of extensional collapse and rifting, with raising the asthenosphere to fill the rift; **(c)** Slab breaks off and rises of hot asthenosphere lead to magmatism; **(d)** Slab sinks away and asthenosphere up wells, which caused common melting of the subducted oceanic crust and induce partial melting to produce a calc-alkaline and alkaline magmatism including high-K calc-alkaline Qattar granitic rocks in ANS.

6. Conclusions

Qattar alkali-feldspar granitoids originated from a highly fractionated rich K calc-alkaline magma source under oxidizing conditions (avg. *log fO2* -14.88). These granitoids show a geochemical signature characteristic of A1-subtype granite, such as slightly peraluminous, highly SiO_2, alkalis (Na_2O+K_2O), Rb, Zr, contents, rich K calc-alkaline magma, and belong to the ferroan granites group with low MgO, CaO, and MnO contents and high FeO^{tot}/ FeO^{tot}+MgO ratios. They have low REE (104.5–123.90 ppm), slight enrichment in LREE $(La/Yb)_N$ =0.32–0.61), negative Eu (Eu/Eu*, 0.10–0.28), and strong negative Ti, Pb, and Sr anomalies (primitive mantel-normalization) indicating magmatic fractional crystallization. They emplaced at depths between 8.33 to 10.57 km, at a temperature of 755.3 °C, and under pressure 2.33-2.95 kbars by

delaminating the lithospheric root and slab break-off. They are highly F-rich differentiated granites hosted by four types of fluorites, varying from sky blue, light-yellow, colorless, and yellow in color. Moreover, these fluorites show a wide range of REE variations and negative Eu anomaly, indicating crystallization temperatures above 200 °C (under reduced or weakly oxidizing conditions) and affected by chemical complexation and physiochemical conditions of REE leaching.

References

[1] R. J. Stern, K. A. Ali, J.-P. Liégeois, P. R. Johnson, W. Kozdroj, and F. H. Kattan, '° Distribution and significance of pre-Neoproterozoic zircons in juvenile Neoproterozoic igneous rocks of the Arabian-Nubian Shield', *American Journal of Science*, vol. 310, no. 9, pp. 791–811, 2010.

[2] M. G. Abdelsalam and R. J. Stern, 'Sutures and shear zones in the Arabian-Nubian Shield', *Journal of African Earth Sciences*, vol. 23, no. 3, pp. 289–310, 1996.

[3] K. C. Condie, E. Belousova, W. L. Griffin, and K. N. Sircombe, 'Granitoid events in space and time: constraints from igneous and detrital zircon age spectra', *Gondwana Research*, vol. 15, no. 3–4, pp. 228–242, 2009.

[4] R. J. Stern, 'Crustal evolution in the East African Orogen: a neodymium isotopic perspective', *Journal of African Earth Sciences*, vol. 34, no. 3–4, pp. 109–117, 2002.

[5] R. J. Stern, 'Arc assembly and continental collision in the Neoproterozoic East African Orogen: implications for the consolidation of Gondwanaland', *Annual review of earth and planetary sciences*, vol. 22, no. 1, pp. 319–351, 1994.

[6] Y. Be'eri-Shlevin, Y. Katzir, and M. Whitehouse, 'Post-collisional tectonomagmatic evolution in the northern Arabian–Nubian Shield: time constraints from ion-probe U–Pb dating of zircon', *Journal of the Geological Society*, vol. 166, no. 1, pp. 71–85, 2009.

[7] Y. Be'eri-Shlevin, Y. Katzir, and J. W. Valley, 'Crustal evolution and recycling in a juvenile continent: oxygen isotope ratio of zircon in the northern Arabian Nubian Shield', *Lithos*, vol. 107, no. 3–4, pp. 169–184, 2009.

[8] R. J. Stern, 'Neoproterozoic crustal growth: the solid Earth system during a critical episode of Earth history', *Gondwana research*, vol. 14, no. 1–2, pp. 33–50, 2008.

[9] D. B. Stoeser and C. D. Frost, 'Nd, Pb, Sr, and O isotopic characterization of Saudi Arabian shield terranes', *Chemical Geology*, vol. 226, no. 3–4, pp. 163–188, 2006.

[10] D. Avigad and Z. Gvirtzman, 'Late Neoproterozoic rise and fall of the northern Arabian–Nubian Shield: the role of lithospheric mantle delamination and subsequent thermal subsidence', *Tectonophysics*, vol. 477, no. 3–4, pp. 217–228, 2009.

[11] M. Z. El-Bialy, 'On the Pan-African transition of the Arabian–Nubian Shield from compression to extension: the post-collision Dokhan volcanic suite of Kid-Malhak region, Sinai, Egypt', *Gondwana Research*, vol. 17, no. 1, pp. 26–43, 2010.

[12] M. Eyal, B. Litvinovsky, B. M. Jahn, A. Zanvilevich, and Y. Katzir, 'Origin and evolution of post-collisional magmatism: coeval Neoproterozoic calc-alkaline and alkaline suites of the Sinai Peninsula', *Chemical Geology*, vol. 269, no. 3–4, pp. 153–179, 2010.

[13] P. R. Johnson *et al.*, 'Late Cryogenian–Ediacaran history of the Arabian–Nubian Shield: a review of depositional, plutonic, structural, and tectonic events in the closing stages of the northern East African Orogen', *Journal of African Earth Sciences*, vol. 61, no. 3, pp. 167–232, 2011.

[14] R. J. Stern and C. E. Hedge, 'Geochronologic and isotopic constraints on late Precambrian crustal evolution in the Eastern Desert of Egypt', *American Journal of Science*, vol. 285, no. 2, pp. 97–127, 1985.

[15] M. F. Akaad and A. M. Noweir, 'Geology and lithostratigraphy of the Arabian Desert orogenic belt of Egypt between latitudes 25°35'S and 26°30'N.', *Inst Appl Geol Jeddah Bull*, vol. 3, pp. 127–135, 1978.

[16] S. EL Gaby, 'Petrochemistry and geochemistry of some granites from Egypt', *Neues Jahrb. Miner. Abh.*, vol. 124, pp. 147–189, 1975.

[17] M. F. El-Ramly and M. K. Akaad, 'The basement complex in the central Eastern Desert of Egypt between latitudes 24 30 and 25 40 N', *Geological Survey of Egypt*, p. 33, 1960.

[18] W. Elwan, S. A. Azzaz, M. R. Balasi, and O. Amer, 'Petrogenesis of Maktali fractionated calc-alkaline younger granitoids, Central Eastern Desert, Egypt', *Arabian Journal of Geosciences*, vol. 12, no. 13, pp. 1–17, 2019.

[19] M. K. Azer, 'Late Ediacaran (605–580Ma) post-collisional alkaline magmatism in the Arabian–Nubian Shield: A case study of Serbal ring-shaped intrusion, southern Sinai, Egypt', *Journal of Asian Earth Sciences*, vol. 77, pp. 203–223, 2013, doi: https://doi.org/10.1016/j.jseaes.2013.08.029.

[20] M. Bielski, E. Jäger, and G. Steinitz, 'The geochronology of Iqna granite (Wadi Kid pluton), southern Sinai', *Contributions to Mineralogy and Petrology*, vol. 70, pp. 159–165, 1979.

[21] A. M. Moghazi, 'Geochemistry and petrogenesis of late Proterozoic plutonic rock suites in the Homrit Waggat and El-Yatima areas, Eastern Desert, Egypt', in *4th International Conference on Geochemistry, Alexandria University, Egypt, Alexandria Egypt, 1999*, 1999, pp. 1–21.

[22] N. M. Mahdy, M. H. Shalaby, H. M. Helmy, A. F. Osman, E. S. H. El Sawey, and E. K. A. Zeid, 'Trace and REE element geochemistry of fluorite and its relation to uranium mineralizations, Gabal Gattar Area, Northern Eastern Desert, Egypt', *Arabian Journal of Geosciences*, vol. 7, pp. 2573–2589, 2014.

[23] O. Amer, S. Kharbish, A. Maged, and F. Khedr, 'Geochemical insight into granite hosted U-rich fluorite, Gabal El-Erediya area, Central Eastern Desert, Egypt: REE geochemical and fluid inclusion aspects', *Arabian Journal of Geosciences*, vol. 14, no. 13, pp. 1–17, 2021.

[24] A. B. Salman, 'New occurrence of uranium mineralization in Gebel Gattar, northern Eastern Desert, Egypt', *Ann. Geol. Surv. Egypt*, vol. 51, pp. 31–34, 1990.

[25] M. L. El Rakaiby and M. H. Shalaby, 'Geology of gebel qattar batholith, central eastern desert, Egypt', *International Journal of Remote Sensing*, vol. 13, no. 12, pp. 2337–2347, 1992.

[26] H. M. Helmy, 'Mineralogy, fluid inclusions and geochemistry of the molybdenum-uranium-fluorite mineralizations, Gebel Gattar area, Eastern Desert, Egypt', in *Intern. Conf. on Geochemistry, Alexandria University*, 1999, pp. 171–198.

[27] A. El-Kammar, A. Salman, and A. Mahdy, 'Geochemical and genetical constraints on rare metals mineralization at the central Eastern Desert of Egypt', *Geochemical Journal*, vol. 35, no. 2, pp. 117–135, 2001.

[28] M. G. El-Feky, 'Mineralogical, REE-geochemical and fluid inclusion studies on some uranium occurrences, Gabal Gattar, Northeastern Desert, Egypt', *Chinese Journal of Geochemistry*, vol. 30, pp. 430–443, 2011.

[29] N. M. Mahdy, B. A. El Kalioubi, C. C. Wohlgemuth-Ueberwasser, M. H. Shalaby, and A. H. El-Afandy, 'Petrogenesis of U-and Mo-bearing A2-type granite of the Gattar batholith in the Arabian Nubian Shield, Northeastern Desert, Egypt: evidence for the favorability of host rocks for the origin of associated ore deposits', *Ore geology reviews*, vol. 71, pp. 57–81, 2015.

[30] A. Dardir and Abu Zeid, 'Geology of the basement rocks between lat. 27 00′ and 27 30′ N, Eastern Desert', *Annals of Geological Survey of Egypt*, vol. 11, pp. 129–159, 1972.

[31] N. M. Mahdy, 'Mineralogical studies and mineral chemistry of some radioactive mineralizations in Gabal Gattar area, Northern Eastern Desert, Egypt', *Ain Shams University, Egypt*, 2011.

[32] M. M. El-Sayed, M. H. Shalaby, and M. A. Hassanen, 'Petrological and geochemical constraints on the tectonomagmatic evolution of the late Neoproterozoic granitoid suites in the Gattar area, north Eastern Desert, Egypt', *Neues Jahrbuch für Mineralogie-Abhandlungen*, pp. 239–275, 2003.

[33] A. Abdel Warith, M. Michalik, and B. H. Ali, 'Fluorine enriched granites: chemical characterization and relation to uranium mineralization', *J Appl Sci*, vol. 6, no. 4, pp. 299–323, 2010.

[34] M. H. Shalaby, 'Structural controls of uranium mineralization at Gabal Gattar, north Eastern Desert, Egypt', in *Egyptian Academy of Sciences*, 1996, pp. 521–536.

[35] G. N. Eby, 'The A-type granitoids: a review of their occurrence and chemical characteristics and speculations on their petrogenesis', *Lithos*, vol. 26, no. 1–2, pp. 115–134, 1990.

[36] J. B. Whalen, K. L. Currie, and B. W. Chappell, 'A-type granites: geochemical characteristics, discrimination and petrogenesis', *Contributions to mineralogy and petrology*, vol. 95, pp. 407–419, 1987.

[37] P. D. Maniar and P. M. Piccoli, 'Tectonic discrimination of granitoids', *Geological society of America bulletin*, vol. 101, no. 5, pp. 635–643, 1989.

[38] A. Streckeisen and R. W. Le Maitre, 'A chemical approximation to the modal QAPF classification of the igneous rocks', 1979.

[39] B. R. Frost, C. G. Barnes, W. J. Collins, R. J. Arculus, D. J. Ellis, and C. D. Frost, 'A geochemical classification for granitic rocks', *Journal of petrology*, vol. 42, no. 11, pp. 2033–2048, 2001.

[40] A. R. Hastie, A. C. Kerr, J. A. Pearce, and S. F. Mitchell, 'Classification of altered volcanic island arc rocks using immobile trace elements: development of the Th–Co discrimination diagram', *Journal of petrology*, vol. 48, no. 12, pp. 2341–2357, 2007.

[41] P. J. Sylvester, 'Post-collisional alkaline granites', *The Journal of Geology*, vol. 97, no. 3, pp. 261–280, 1989.

[42] M. A. Hassan and A. H. Hashad, 'Precambrian of Egypt In: Said R (ed) The geology of Egypt', *Balkema, Rotterdam*, pp. 201–245, 1990.

[43] D. B. Clarke, 'The mineralogy of peraluminous granites; a review', *The Canadian Mineralogist*, vol. 19, no. 1, pp. 3–17, 1981.

[44] J. N. Rossi, A. J. Toselli, M. A. Basei, A. N. Sial, and M. Baez, 'Geochemical indicators of metalliferous fertility in the Carboniferous San Blas pluton, Sierra de Velasco, Argentina', *Geological Society, London, Special Publications*, vol. 350, no. 1, pp. 175–186, 2011.

[45] P. Blevin, 'Metallogeny of granitic rocks', in *The Ishihara Symposium, Granites and Associated Metallogenesis*, 2003, pp. 5–8.

[46] G. Tischendorf, 'Geochemical and petrographic characteristics of silicic magmatic rocks associated with rare-metal mineralization', *Metallization Associated with Acid Magmatism, 2*, pp. 41–98, 1977.

[47] S.-S. Sun and W. F. McDonough, 'Chemical and isotopic systematics of oceanic basalts: implications for mantle composition and processes', *Geological Society, London, Special Publications*, vol. 42, no. 1, pp. 313–345, 1989.

[48] A. R. Drysdall, N. J. Jackson, C. R. Ramsay, C. J. Douch, and D. Hackett, 'Rare element mineralization related to Precambrian alkali granites in the Arabian Shield', *Economic Geology*, vol. 79, no. 6, pp. 1366–1377, 1984.

[49] J. Tarney and C. E. Jones, 'Trace element geochemistry of orogenic igneous rocks and crustal growth models', *Journal of the Geological Society*, vol. 151, no. 5, pp. 855–868, 1994.

[50] G. N. Eby, 'Chemical subdivision of the A-type granitoids: petrogenetic and tectonic implications', *Geology*, vol. 20, no. 7, pp. 641–644, 1992.

[51] S. Jung and J. A. Pfänder, 'Source composition and melting temperatures of orogenic granitoids: constraints from CaO/Na2O, Al2O3/TiO2 and accessory mineral saturation thermometry', *European Journal of Mineralogy*, vol. 19, no. 6, pp. 859–870, 2007.

[52] B. W. Chappell, C. J. Bryant, D. Wyborn, A. J. R. White, and I. S. Williams, 'High-and low-temperature I-type granites', *Resource Geology*, vol. 48, no. 4, pp. 225–235, 1998.

[53] X.-M. Yang, 'Estimation of crystallization pressure of granite intrusions', *Lithos*, vol. 286, pp. 324–329, 2017.

[54] J. S. Huebner and M. Sato, 'The oxygen fugacity-temperature relationships of manganese oxide and nickel oxide buffers', *American Mineralogist: Journal of Earth and Planetary Materials*, vol. 55, no. 5–6, pp. 934–952, 1970.

[55] D. R. Wones, 'Significance of the assemblage titanite+ magnetite+ quartz in granitic rocks', *American Mineralogist*, vol. 74, no. 7–8, pp. 744–749, 1989.

[56] B. Chen, X. Ma, and Z. Wang, 'Origin of the fluorine-rich highly differentiated granites from the Qianlishan composite plutons (South China) and implications for polymetallic mineralization', *Journal of Asian Earth Sciences*, vol. 93, pp. 301–314, 2014.

[57] M. Bau, 'Controls on the fractionation of isovalent trace elements in magmatic and aqueous systems: evidence from Y/Ho, Zr/Hf, and lanthanide tetrad effect', *Contributions to Mineralogy and Petrology*, vol. 123, no. 3, pp. 323–333, 1996.

[58] B. Jahn, F. Wu, R. Capdevila, F. Martineau, Z. Zhao, and Y. Wang, 'Highly evolved juvenile granites with tetrad REE patterns: the Woduhe and Baerzhe granites from the Great Xing'an Mountains in NE China', *Lithos*, vol. 59, no. 4, pp. 171–198, 2001.

[59] W. Irber, 'The lanthanide tetrad effect and its correlation with K/Rb, Eu/Eu∗, Sr/Eu, Y/Ho, and Zr/Hf of evolving peraluminous granite suites', *Geochimica et Cosmochimica Acta*, vol. 63, no. 3–4, pp. 489–508, 1999.

[60] Z. Zhenhua *et al.*, 'Controls on the REE tetrad effect in Evidence from the Qianlishan and Baerzhe granites: Granites, China', *Geochemical journal*, vol. 36, no. 6, pp. 527–543, 2002.

[61] B. Chen and B. Jahn, 'Genesis of post-collisional granitoids and basement nature of the Junggar Terrane, NW China: Nd–Sr isotope and trace element evidence', *Journal of Asian Earth Sciences*, vol. 23, no. 5, pp. 691–703, 2004.

[62] R. A. Rich, H. D. Holland, and U. Petersen, 'Hydrothermal uranium deposits', 1977.

[63] C. Peiffert and M. Cuney, 'Uranium in granitic magmas: Part 2. Experimental determination of uranium solubility and fluid-melt partition coefficients in the uranium oxide-haplogranite-H2O-NaX (X= Cl, F) system at 770 C, 2 kbar', *Geochimica et cosmochimica acta*, vol. 60, no. 9, pp. 1515–1529, 1996.

[64] B. O. Mysen, G. D. Cody, and A. Smith, 'Solubility mechanisms of fluorine in peralkaline and meta-aluminous silicate glasses and in melts to magmatic temperatures', *Geochimica et Cosmochimica Acta*, vol. 68, no. 12, pp. 2745–2769, 2004.

[65] A. Chabiron, M. Cuney, and B. Poty, 'Possible uranium sources for the largest uranium district associated with volcanism: the Streltsovka caldera (Transbaikalia, Russia)', *Mineralium Deposita*, vol. 38, pp. 127–140, 2003.

[66] L. Z.-X. L. Gong-Xu, 'The simulation test of granite uranium mineralization', *Earth Science Frontiers*, vol. 16, no. 1, p. 99, 2009.

[67] A. Maged, S. Kharbish, I. S. Ismael, and A. Bhatnagar, 'Characterization of activated bentonite clay mineral and the mechanisms underlying its sorption for ciprofloxacin from aqueous solution', *Environmental Science and Pollution Research*, vol. 27, pp. 32980–32997, 2020.

[68] H. Keppler and P. J. Wyllie, 'Partitioning of Cu, Sn, Mo, W, U, and Th between melt and aqueous fluid in the systems haplogranite-H2O− HCl and haplogranite-H2O− HF', *Contributions to Mineralogy and Petrology*, vol. 109, no. 2, pp. 139–150, 1991.

[69] P. Möller, P. P. Parekh, and H.-J. Schneider, 'The application of Tb/Ca-Tb/La abundance ratios to problems of fluorspar genesis', *Mineralium Deposita*, vol. 11, no. 1, pp. 111–116, 1976.

[70] M. Fleischer, 'The lanthanide elements in fluorite', *Indian Mineral*, vol. 10, pp. 36–39, 1969.

[71] M. Bau, 'Rare-earth element mobility during hydrothermal and metamorphic fluid-rock interaction and the significance of the oxidation state of europium', *Chemical Geology*, vol. 93, no. 3–4, pp. 219–230, 1991.

[72] P. Moeller and E. Holzbecher, 'Eu anomalies in hydrothermal fluids and minerals: A combined thermochemical and dynamic phenomenon', in *Hans-Jürgen-Behr-Festschrift*, 1998, pp. 73–84.

[73] P. Möller, M. Bau, P. Dulski, and V. Lüders, 'REE and yttrium fractionation in fluorite and their bearing on fluorite formation', in *Proc 9th Quadr IAGOD Symp*, 1998, pp. 575–592.

[74] G. Schwinn and G. Markl, 'REE systematics in hydrothermal fluorite', *Chemical Geology*, vol. 216, no. 3–4, pp. 225–248, 2005.

[75] G. T. Hill, A. R. Campbell, and P. R. Kyle, 'Geochemistry of southwestern New Mexico fluorite occurrences implications for precious metals exploration in fluorite-bearing systems', *Journal of Geochemical Exploration*, vol. 68, no. 1–2, pp. 1–20, 2000.

[76] F. Wu, D. Sun, H. Li, B. Jahn, and S. Wilde, 'A-type granites in northeastern China: age and geochemical constraints on their petrogenesis', *Chemical Geology*, vol. 187, no. 1–2, pp. 143–173, 2002.

[77] X.-H. Li *et al.*, 'U–Pb zircon, geochemical and Sr–Nd–Hf isotopic constraints on age and origin of Jurassic I-and A-type granites from central Guangdong, SE China: a major igneous event in response to foundering of a subducted flat-slab?', *Lithos*, vol. 96, no. 1–2, pp. 186–204, 2007.

[78] B. Sperner, F. Lorenz, K. Bonjer, S. Hettel, B. Müller, and F. Wenzel, 'Slab break-off–abrupt cut or gradual detachment? New insights from the Vrancea Region (SE Carpathians, Romania)', *Terra Nova*, vol. 13, no. 3, pp. 172–179, 2001.

[79] F. Espinoza *et al.*, 'Petrogenesis of the Eocene and Mio–Pliocene alkaline basaltic magmatism in Meseta Chile Chico, southern Patagonia, Chile: Evidence for the participation of two slab windows', *Lithos*, vol. 82, no. 3–4, pp. 315–343, 2005.

[80] K. C. Condie, 'Archean magmatism and crustal thickening', *Geological Society of America Bulletin*, vol. 84, no. 9, pp. 2981–2992, 1973.

[81] M. Cuney, 'The extreme diversity of uranium deposits', *Mineralium Deposita*, vol. 44, no. 1, p. 3, 2009.

[82] F. Barker, 'Trondhjemite: definition, environment and hypotheses of origin', in *Developments in petrology*, Elsevier, 1979, pp. 1–12.

[83] D. A. C. Manning, 'The effect of fluorine on liquidus phase relationships in the system Qz-Ab-Or with excess water at 1 kb', *Contributions to Mineralogy and Petrology*, vol. 76, pp. 206–215, 1981.

[84] W. Johannes and F. Holtz, *Petrogenesis and experimental petrology of granitic rocks*, vol. 22. Springer Science & Business Media, 2012.

[85] N. W. Rogers, C. J. Hawkesworth, D. P. Mattey, and R. S. Harmon, 'Sediment subduction and the source of potassium in orogenic leucitites', *Geology*, vol. 15, no. 5, pp. 451–453, 1987.

[86] M. G. Abdelsalam, J.-P. Liégeois, and R. J. Stern, 'The Saharan Metacraton', *Journal of African Earth Sciences*, vol. 34, no. 3, pp. 119–136, 2002, doi: https://doi.org/10.1016/S0899-5362(02)00013-1.

[87] H. A. Eliwa *et al.*, 'SIMS zircon U–Pb and mica K–Ar geochronology, and Sr–Nd isotope geochemistry of Neoproterozoic granitoids and their bearing on the evolution of the north Eastern Desert, Egypt', *Gondwana Research*, vol. 25, no. 4, pp. 1570–1598, 2014.

[88] J. H. Davies and F. von Blanckenburg, 'Slab breakoff: a model of lithosphere detachment and its test in the magmatism and deformation of collisional orogens', *Earth and planetary science letters*, vol. 129, no. 1–4, pp. 85–102, 1995.

[89] E. S. Farahat, H. A. Mohamed, A. F. Ahmed, and M. M. El Mahallawi, 'Origin of I-and A-type granitoids from the Eastern Desert of Egypt: implications for crustal growth in the northern Arabian–Nubian Shield', *Journal of African Earth Sciences*, vol. 49, no. 1–2, pp. 43–58, 2007.

[90] B. Bonin, 'Do coeval mafic and felsic magmas in post-collisional to within-plate regimes necessarily imply two contrasting, mantle and crustal, sources? A review', *Lithos*, vol. 78, no. 1–2, pp. 1–24, 2004.

[91] E. S. Farahat and M. K. Azer, 'Post-collisional magmatism in the northern Arabian-Nubian Shield: the geotectonic evolution of the alkaline suite at Gebel Tarbush area, south Sinai, Egypt', *Geochemistry*, vol. 71, no. 3, pp. 247–266, 2011.

[92] S. A. Abu El-Magd, A. Maged, and H. I. Farhat, 'Hybrid-based Bayesian algorithm and hydrologic indices for flash flood vulnerability assessment in coastal regions: machine learning, risk prediction, and environmental impact', *Environmental Science and Pollution Research*, vol. 29, no. 38, pp. 57345–57356, 2022.

[93] A. Abdelnasser, L. Khedr, S. Kharbish, B. Zoheir, and S. Zamzam, 'Sulfide disseminations and hydrothermal alteration haloes in the Gabal Monqul area, Egypt: Field, mineralogical, and remote sensing studies', *Journal of African Earth Sciences*, vol. 199, p. 104830, Mar. 2023, doi: 10.1016/j.jafrearsci.2023.104830.

View publication stats

ResearchGate

See discussions, stats, and author profiles for this publication at: https://www.researchgate.net/publication/371711933

Petrogenesis of fractionated calc-alkaline A-type granites and related fluorite, North Eastern Desert, Egypt

Article *in* Frontiers in Scientific Research and Technology · June 2023

DOI: 10.21608/fsrt.2023.209091.1092

CITATION
1

READS
82

3 authors:

Omar Amer
Zagazig University
10 PUBLICATIONS **33** CITATIONS

SEE PROFILE

Sherif Kharbish
Suez University
67 PUBLICATIONS **802** CITATIONS

SEE PROFILE

Ali Maged
Lappeenranta – Lahti University of Technology LUT
19 PUBLICATIONS **354** CITATIONS

SEE PROFILE

All content following this page was uploaded by Omar Amer on 22 June 2023.

The user has requested enhancement of the downloaded file.